

Modeling the Influence of Carbon Spheres on the Porosity of SOFC Anode Materials

Bahman Amini Horri, Cordelia Selomulya, and Huanting Wang[†]

Department of Chemical Engineering, Monash University, Clayton, Victoria, 3800, Australia

The influence of fabrication pressure and other ceramic processing variables, including volumetric loading fraction and the particle size ratio of pore-forming agents, on the porosity of fabricated ceramic anodes, was investigated using an integrated experimental approach with mathematical modeling to differentiate the impacts of each parameter. Despite historic observation of the properties of ceramic bodies, to date, there is a lack of available models to accurately interpret the ceramic properties as a function of the processing variables. Herein, we focus on the open porosity of the solid oxide fuel cell anode prepared from NiO/YSZ (nickel oxide/yttria stabilized zirconia) as the ceramic powder and using CMS (carbon microspheres) as a pore-forming agent. A range of pore-former volumetric blend ratios (4.4%–44.6%) and different particle size ratios between NiO/YSZ and CMS (11.27, 4.29, and 0.26) were used, whereas the influence of the applied uni-axial fabrication pressure on the open porosity of sintered anode was studied in a range of atmospheric pressure up to 40 MPa. A good agreement was observed between the proposed model and the experimental data, implying that the approach could be used to determine the significant processing parameters to fabricate ceramics with desired porosity. The model could also be used to interpret the physical basis of pore formation when using a pore-forming agent in a fabricated porous ceramic body.

I. Introduction

CONVENTIONALLY, the term “porosity” as a microstructural feature has been used to describe the degree of porous nature and to quantitate the void volume of ceramic bodies. Although a variety of factors such as particle size, shape, nature (polycrystalline or composite), surface roughness, chemical properties of crystals, fabrication processing requirements, sintering parameters, morphology, and green density impact the microstructure of fabricated-ceramic bodies, porosity is the dominant factor affecting the properties of ceramic bodies.¹ In general, the presence of porosity degrades mechanical strength, elastic modulus, and ionic-, electronic-, and thermal-conductivity of ceramic bodies.^{2–4} In particular, the performance of electrodes in solid oxide fuel cells depends on the availability of surface area for reaction and the ability of reactants to reach the reaction sites.^{5,6} To increase the performance of the ceramic substrate used as the electrode in solid oxide fuel cells (SOFCs), an optimal porosity level is required to provide sufficient gas permeability, suitable electrical conductivity, enough mechanical strength, high electrochemical catalytic activity, low Ohmic polarization (dielectric break-down voltage), and good compatibility with other fuel-cell components.^{7–10}

Tortuosity is another microstructural parameter in controlling the electrochemical performance of the electrode in SOFCs.¹¹ The tortuosity affects the rate of diffusional transport and thus concentration polarization in the porous ceramic electrodes.^{12,13} In an electrode-supported SOFC, the electrode layer should be thick enough to mechanically support the cell. With a thicker electrode, the concentration polarization is increased in the cell.¹⁴ For this reason, the tortuosity of a porous ceramic should be statistically controlled by tuning calcination and sintering conditions or by changing the particle size of starting materials.¹⁵

Many ceramic bodies formed from powders may intrinsically contain some degrees of porosity due to incomplete densification depending on both the fabrication process and the selected parameters.^{5,16} In the fabrication of the ceramic membranes, catalyst supports, or electrodes of the solid oxide fuel cells, a conventional way to increase the porosity of ceramic substrates is by adding a reasonable amount of a pore-forming agent (PFA) e.g., synthetic polymers, natural biopolymers, or carbon-based materials that could be burnt out during the sintering steps.^{17,18} However, the ability to fabricate the ceramic substrates with desired porosity and controlled microstructural properties is still a challenge.¹⁹

Compaction of powders is a shape-forming technique that has been widely used in ceramics and in other fields such as metallurgy, pharmaceuticals, and civil engineering.²⁰ Mathematical equations describing compaction are often used to adjust the required density of fabricated ceramic bodies in both isostatic and uniaxial die pressing modes. Most of these equations have been developed empirically to fit the experimental data due to the limited theoretic basis.²¹ A summary of more frequently used compaction equations is shown in Table I. The first compaction model [Eq. (1)] proposed by Walker correlated the relative volume of compacted powder against the logarithm of applied axial pressure.²² Balshin applied the concepts of fluid mechanics to justify Walker's equation by theoretic parameters, such as the pressing modulus and the coefficient of deformability.²³ Heckel²⁴ and Kawakita and Ludde²⁵ models [Eqs. (3) and (4)] have been frequently referred to in the pharmaceutical and metallurgy fields due to their good compatibility with the elastic compression phase, more practical relevance, and possibility to measure the yield pressure. Bruch [Eq. (5)] was the first who applied compaction curves to interpret ceramic (alumina powder) consolidation behavior.²⁶ A summary of early compaction equations up to 1983 has been listed by MacLeod.²⁷ More recent overviews of compaction equations have been discussed by Celik²⁸ and Sonnergaard.²⁹

Comparably, the influence of particle size and particle size distribution on the compaction properties has been given less consideration in literature. Dalla Valle³⁰ was the first who introduced the concept of particle pressure diffusion, meaning that small particles tend to diffuse into the void spaces between large particles as a result of increase in applied pressure. Cooper and Eaton³¹ used the same theory to propose an empirical model [Eq. (6)] to describe the compaction behavior of four different ceramic powders. The influence of

J. Stevenson—contributing editor

Manuscript No. 30243. Received August 29, 2011; approved November 28, 2011.

[†]Author to whom correspondence should be addressed. e-mail: huanting.wang@monash.edu

Table I. Summary of Different Compaction Models and Their Applications in Original Form

Model	Correlation [†]	Application Remarks	Ref.
Walker (1923)	$V_r = a_1 - b_1 \cdot \text{Log}(R)$	Fine powders (Calcium Carbonate)	22
Balshin (1938)	$\text{Log}(p) = -L \cdot V_r + c$	Metallic powders	23
Heckel (1961)	$\text{Ln}\left(\frac{1}{1 - \rho_r}\right) = a_2 P + b_2$	Pharmaceutical and metallurgy powders	24
Kawakita & Ludde (1971)	$P\left(\frac{V_0}{V_0 - V}\right) = \frac{1}{a_3 \cdot b_3} + \frac{P}{a_3}$	Pharmaceutical powders	25
Bruch (1967)	$\rho_r = a_4 \cdot \text{Ln}(P) + b_4$	Ceramic powders	26
Cooper and Eaton (1962)	$\frac{V_0 - V}{V_0 - V_s} = a_5 \text{Exp}\left(-\frac{K_1}{P}\right) + b_5 \text{Exp}\left(-\frac{K_2}{P}\right)$	Ceramic powders	31
Yu & Gu (1992)	$\text{Ln}\left(\text{Ln}\left(\frac{\epsilon_0}{\epsilon}\right)\right) = \text{Ln}\left(\frac{a_6}{1 + b_6}\right) + (1 + b_6) \cdot \text{Ln}(P)$	Fine powder (river sand)	37

[†]Symbols: $a_1, a_2, a_3, a_4, a_5, a_6, b_1, b_2, b_3, b_4, b_5, b_6, k_1, k_2$: Model coefficient (determined experimentally via curve fitting); c , The coefficient of deformability (determined experimentally); L , The pressing modulus analogous to Young's modulus (determined experimentally); P , Applied pressure in compression (MPa); R , Resistance to compression (kg/cm^2); V_0 , Volume of powder at zero (relative) pressure (m^3); V_r , Relative volume of the powder (the ratio of apparent volume to the skeletal volume, dimensionless); ϵ, ϵ_0 , Porosity and initial porosity at ambient pressure, respectively (dimensionless); ρ_r , Relative density of the powder (the ratio of apparent density to the skeletal density, dimensionless).

particle size on the pressure modulus was modeled in other works.^{32–34} The effect of particle size distribution by considering the packing efficiency as a function of forming pressure was modeled by Zheng *et al.*³⁵ The influence of particle size range on the deformability of ceramic powder was modeled in another paper, showing that an increase in the particle size caused a decrease in the brittle fracture stress.³⁶ Yu and Gu³⁷ investigated the influence of particle size distribution on the compaction of cohesion-less powders and modeled the densification process using a porosity-pressure correlation [Eq. (8)]. The most recent work dealing with the compaction modeling has used the discrete element method to describe the behavior of aggregated ceramic powders.³⁸ Despite various studies concerning porosity and its effects on the properties of ceramic bodies, what is currently lacking is a reliable mathematical model to accurately predict porosity as a function of the ceramic processing variables.^{39–43}

This work focused on developing a mathematical model of the porosity of porous ceramic substrates, by quantitating the influence of pore-forming agent and ceramic particle properties such as blend ratio, size ratio, and the uni-axial pressure. A range of pore-former blend ratio, particle size ratio, and applied uniaxial pressure were selected as the processing parameters. The model was developed using NiO/YSZ (nickel oxide/yttria stabilized zirconia) as an example of the ceramic powders widely used in the fabrication of solid oxide fuel cells. The experimental results were obtained using spherical carbon particles with three different diameters as the pore-forming agent to minimize the effects of pore-former shape factor on the final porosity. The proposed equations can be specially used to assist in the fabrication of porous ceramic substrates with a desired open porosity, by adjusting these processing parameters. Also, this compaction model can be generally used to understand the dominant process parameters and the physical basis of pore formation inside a porous ceramic body when a pore-forming agent is used.

II. Experimental Procedure

(1) Preparation and Characterization of Ceramic Powders and Pore-Forming Agent

To prepare the ceramic powders for this study, nickel carbonate-basic hydrate, BNC ($\text{NiCO}_3 \cdot 2\text{Ni}(\text{OH})_2 \cdot x\text{H}_2\text{O}$, MW = 304.12 g/mol; Sigma-Aldrich, Sydney, Australia) and yttria stabilized zirconium (IV) oxide, YSZ ($\text{ZrO}_2 \cdot \text{Y}_2\text{O}_3$, 99.9%, MW = 123.22 g/mol; Sigma-Aldrich) were used as the source of ceramic materials. About 300 g of BNC was thermally decomposed at 500°C for 4 h. NiO/YSZ ceramic composite was prepared by dispersing the prepared NiO and YSZ powders into ethanol at the mass ratio of 60:40. The resulting suspension was then ball-milled with zirconia balls (5 mm) for 24 h at 80 rpm. Subsequently, the suspension was dried at around 80°C for 24 h. The prepared NiO/YSZ ceramic powder was characterized using a X-ray diffraction method (Phillips 1140 diffractometer, Philips Co., Eindhoven, The Netherlands).

In this study, carbon micro-spheres (CMS) were used as the pore-forming agent. They were prepared using hydrothermal treatment of sugar according to the method described elsewhere.⁴⁴ Here, processing parameters such as the hydrothermal treatment time and sugar concentration were used as the main controlling factors affecting the spherules diameters. Table sugar (Merryfield white sugar, 100% Australian pure) as the carbon precursor was dissolved into distilled water as the solvent. Three different CMSs (referred to as CMS1, 2, and 3) with different diameters were prepared using sugar solutions with different concentrations of 2.055, 1.233, and 0.616 mol/L. The sugar solutions were filled in separate Teflon autoclaves and placed in an oven at the same temperature of 190°C for 6.5, 2, and 2.5 h, respectively.

The morphology of the prepared CMSs and NiO/YSZ were examined using scanning electron microscopy (JEOL JSM-840A, JEOL Ltd., Tokyo, Japan). The particles size distributions of the prepared powders were measured using laser scattering method (Mastersizer 2000; Malvern Instruments

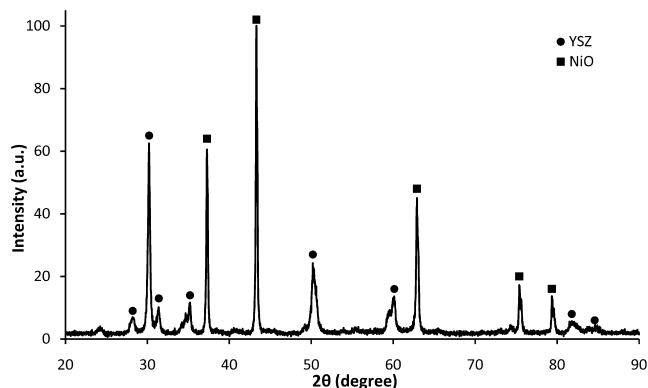


Fig. 1. XRD pattern of prepared NiO/YSZ.

Ltd., Worcestershire, U.K.). The particle density was determined using a helium pycnometric technique (AccuPyc-1330 pycnometer; Micromeritics Instrument Corp., Norcross, GA).

(2) Sample Preparation and Characterization

To study the effects of volumetric fraction of the pore-forming agent in the ceramic powder, five different samples containing 1, 2.5, 5, 10, and 15 wt% of the prepared CMSs with three different average diameter ranges (CMS1: 11.54 μm , CMS2: 4.39 μm , and CMS3: 0.27 μm) were mixed with the prepared NiO/YSZ (a total of 15 samples). Wet ball-milling method in ethanol medium (with zirconia balls of 3 mm and running time of 5 min) was used to mix the resulting suspension. To ensure enough mechanical strength of the system for compression, polyvinyl alcohol, 20 wt% of PVA ($-\text{CH}_2\text{CH}(\text{OH})-$, MW = 31000–50000 g/mol; Sigma-Aldrich) in deionized water was used as the binder. The PVA solution was added to the prepared ceramic suspensions in a ratio of 0.5 wt% of the total ceramic powders. The final suspensions were finally dried in an oven at around 60°C for 48 h.

The prepared ceramic powders were compressed under a constant pressure of 5 MPa to make similar disks with diameters of 10 mm, using a desktop powder pressing machine (model: FY-24-A; MTI Corporation). To study the effect of applied uniaxial compression pressure on the porosity, seven additional samples were prepared without the pore-former under different pressures of 1, 2.5, 5, 10, 20, 30, and 40 MPa for comparison. The porosity of powder was measured separately.

All prepared samples were sintered in air at 1400°C for 5 h and then reduced at 800°C for 3 h using a hydrogen stream (at around 40 cm^3/min). The CMSs in the prepared samples were totally burnt out during the sintering step. The porosity and pore-size distribution of the produced disks were investigated using a mercury intrusion porosimeter (AutoPore III; Micrometric Instrument Corporation).

(3) Data Analysis Method

MS Excel was used to fit and plot the curves. To relate the parameters of each model to the sample properties and data, stepwise multiple linear and nonlinear regression analyses were performed based on the Levenberg–Marquardt (L–M) algorithm. For each model, the goodness of fit was statistically determined using the coefficient of determination (R^2) and the Root of Mean Squared Errors (RMSE).

III Results and Discussion

(1) Characterization and Microstructure of the Prepared Ceramic and Pore-Former Powders

Figure 1 shows the XRD pattern of the prepared NiO/YSZ powder. The SEM images of the prepared NiO/YSZ and also CMSs are shown in Fig. 2(a)–(d). Figure 3 shows the particle

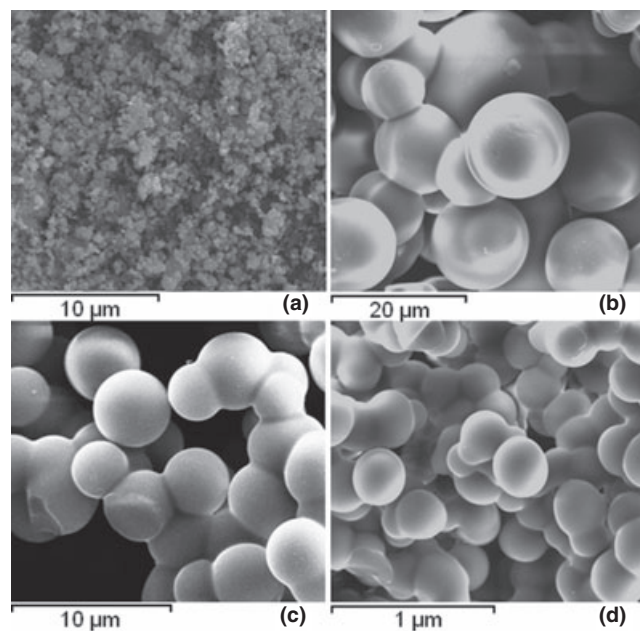


Fig. 2. SEM image of prepared ceramic powder and pore-former. (a) NiO/YSZ, (b) CMS1, (c) CMS2, and (d) CMS3.

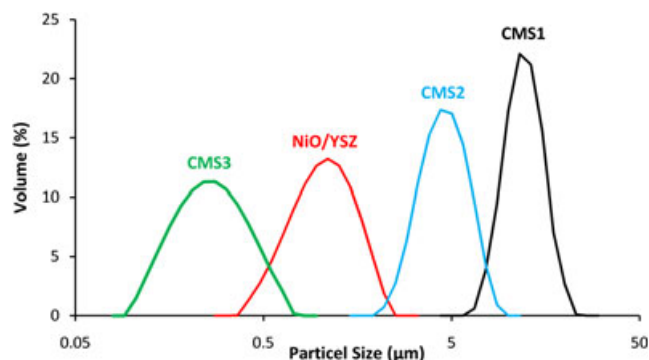


Fig. 3. Particle size distribution for the prepared ceramic and pore-former powders.

Table II. Particle Size Distribution Data

Particle size parameter [†] (μm)	NiO/YSZ	CMS1	CMS2	CMS3
$D(0.1)$	0.566	8.267	2.891	0.137
$D(0.5)$	0.972	11.245	4.240	0.242
$D(0.9)$	1.563	15.103	6.106	0.433
Surface weighted mean diameter	0.887	10.935	4.047	0.222
Volume weighted mean diameter	1.024	11.539	4.390	0.266

[†]The particle size parameters reported using Malvern instrument has less than $\pm 1\%$ error.

size distribution for the prepared powders. Each powder was dispersed in distilled water before particle size measurement, and the results were presented in term of equivalent volume-averaged diameters. The prepared powders showed unimodal distributions in the particle size range (Fig. 3), with detailed data shown in Table II.

(2) Porosity Measurement Results

After sintering and reduction steps, all prepared samples were subjected to the volumetric porosity and the pore-size distribution measurements. The experimental values of samples porosities due to the applied uniaxial pressure (without

Table III. Volumetric Porosity of NiO/YSZ Ceramic Samples (Without Pore-Former) as a Function of Applied Uniaxial Pressure

Applied uniaxial pressure (MPa)	Volumetric porosity [†] , ε (%)
0	59.25
1	31.89
2.5	26.87
5	23.52
10	22.62
20	22.12
30	22.02
40	21.81

[†]Porosity measurement average error: $\pm 1\%$.

Table IV. Volumetric Porosity of NiO/YSZ Ceramic Samples (with Pore-Former) as a Function of Particle Size Ratio and the Blend Ratio of Pore-Former at a Pressure of 5 MPa

Pore-former loading fraction		Volumetric percentage porosity [†] at different mean particle size ratio		
wt%	vol% (Blend ratio, ζ)	$\lambda = 11.268$	$\lambda = 4.287$	$\lambda = 0.260$
0	0	23.52	23.52	23.52
1	4.40	33.01	31.87	29.02
2.5	10.46	37.49	35.18	31.07
5	19.33	42.41	39.53	33.85
10	33.60	51.05	47.24	39.17
15	44.56	61.18	55.46	45.4

[†]Porosity measurement average error: $\pm 1\%$.

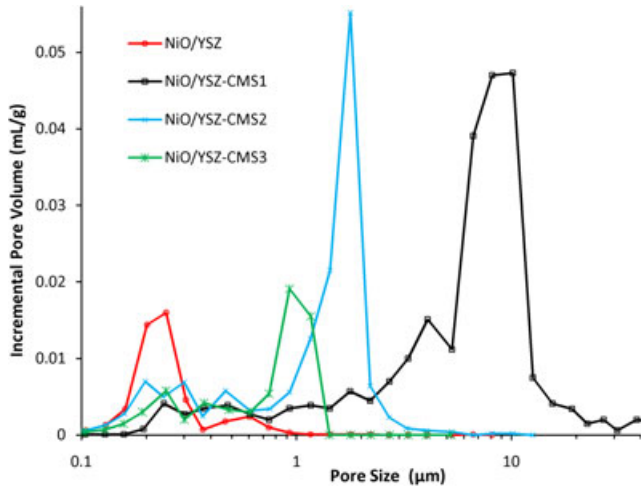


Fig. 4. Pore-size distribution measured by mercury porosimeter for prepared samples at 5 MPa and 15 wt% of added CMS).

pore-former) and the effects of both particle size and loading fraction of the pore-former (CMSs) are presented in Tables III and IV, respectively. Porosity was shown to decrease with lower particle size ratio or the loading fraction of the added CMSs as the pore-former. Figure 4 shows the pore-size distribution of the prepared samples with and without pore-former. According to Fig. 4, the pore-size formed in each sample is compatible with particle size of the applied pore-former. For the sample made by CMS3, the pores formed inside the fabricated ceramic body shows a bigger size (around 1 μm) due to presence of bigger particles and agglomeration of CMS particles in the ceramic substrate.

(3) Porosity Modeling and Analysis

As discussed in previous studies,^{7,45–48} the size, shape, and quantity of the pore-formers significantly influence the micro-

structure, porosity, and pore-size distribution of ceramic substrates. To study the effects of the pore-former, the following process parameters were investigated in this work:

1. The applied uniaxial pressure (P) as used in the powder compaction shape-forming technique.
2. The blend ratio (ζ) which is the volumetric fraction of the pore-forming agent in the total ceramic material and is expressed as:

$$\zeta = \frac{V_p}{V_p + V_c} = \frac{X_p}{X_p + \frac{\rho_p}{\rho_c}} \quad (8)$$

where V_p , and V_c are the skeletal volumes of pore-former and ceramic powder, respectively; X_p is the weight ratio of pore-former in ceramic powder $X_p = \frac{m_p}{m_c}$, and ρ_p , and ρ_c are the skeletal densities of pore-former and ceramic powder, respectively. In this study, the measured values of ρ_p and ρ_c are 1.373 and 6.253 g/cm^3 , respectively.

3. The size ratio (λ) which is the ratio of the volumetric average particle size of pore-forming agent and ceramic particles.

(A) *Effect of Fabrication Pressure:* A predictive porosity model must satisfy two important boundary conditions. First, the predicted porosity must approach the powder porosity as the applied pressure decreases to atmospheric pressure. Secondly, the porosity predicted by a model must approach zero as the applied pressure approaches infinity.^{25,37,49} These conditions can be expressed as:

$$\lim_{P \rightarrow P_a} \varepsilon = \varepsilon_0 \quad (9)$$

$$\lim_{P \rightarrow \infty} \varepsilon = 0 \quad (10)$$

where ε and ε_0 are porosity and powder porosity at ambient pressure, respectively. All powders and fabricated porous materials contain both solid and void fractions. The dimensionless relationship between porosity (void volume fraction) and solid volume fraction (ϕ) is usually expressed as:

$$\varepsilon = 1 - \phi = 1 - \frac{V_s}{V} \quad (11)$$

where V_s and V are the skeletal (apparent) volume and the bulk (envelop) volume of the porous solid (or powder), respectively.⁵⁰ For a compaction process, application of the work done in a cylinder-piston system according to thermodynamic definition of work can be written as:

$$dW = v \cdot dP - Pdv \quad (12)$$

In Eq. (12), W is the total work required for a piston displacement, v is the specific volume of the material inside the cylinder, and P is the applied uniaxial pressure. By dividing the volumes in Eq. (11) by the total mass of solid, a relationship for the bulk specific volume can be written as:

$$v = \frac{v_s}{1 - \varepsilon} \quad (13)$$

where v and v_s are the bulk and skeletal specific volumes, respectively. By substituting Eq. (13) to Eq. (12) and integrating the resulting equation for any piston displacement during a reversible and adiabatic compaction process at a constant pressure, the following equation can be expressed as:

$$W_p = P \cdot v_s \cdot \left[\frac{1}{1 - \varepsilon_0} - \frac{1}{1 - \varepsilon} \right] \quad (14)$$

where W_p is the work done by exerting the uniaxial pressure for compaction of the solid particles. Equation (14) can be rearranged as Eq. (15) for porosity, by introducing a correlation for W_p :

$$\varepsilon = 1 - \frac{1}{\frac{1}{1-\varepsilon_0} - \frac{W_p}{P \cdot v_s}} \quad (15)$$

Compaction process of solid particles in a cylinder-piston system involves several densification sequences that caused some difficulties in getting a direct theoretic expression for W_p . Depending on the powder types and properties, those sequences can be summarized as elastic deformation, plastic deformation, and particle fragmentation.^{28,51,52}

To find a suitable correlation for the pressure work (W_p), Eq. (14) was used to calculate the values of W_p according to the experimental data reported in Table III (porosity versus the applied uniaxial pressure). Curve fitting analysis was used to correlate the equivalent pressure work in terms of both porosity (ε) and the powder porosity (ε_0), as a function of pressure. Figure 5 shows the plot of the experimental values of the pressure work in terms of $\frac{W_p}{P \cdot v_s}$ (as used in Eq. 15) versus pressure difference ($P - P_a$). The following equation was found to satisfy the experimental data from this work:

$$\frac{W_p}{P \cdot v_s} = C \left[A \frac{P - P_a}{P} + (1 - A) \left(1 - \text{Exp} \left(-\frac{P - P_a}{B} \right) \right) \right] \quad (16)$$

where A , B , and C are the model coefficients. To express a model for porosity, Eq. (16) was substituted into Eq. (15), and consequently the resulting equation must satisfy the boundary conditions for general porosity models, i.e., Eqs. (7) and (10). The porosity equation satisfies the first boundary condition, showing that as the pressure difference approaches zero, the porosity approaches the powder porosity (ε_0). The second boundary condition can be applied using the following:

$$\begin{aligned} \lim_{P \rightarrow \infty} \varepsilon &= \lim_{P \rightarrow \infty} 1 \\ &= \frac{1}{\frac{1}{1-\varepsilon_0} - C \left[A \frac{P - P_a}{P} + (1 - A) \left(1 - \text{Exp} \left(-\frac{P - P_a}{B} \right) \right) \right]} \\ &= 0 \end{aligned} \quad (17)$$

which implies that C takes the value of $\frac{\varepsilon}{1-\varepsilon_0}$. By substituting the corresponding expression for C , the proposed equation for porosity becomes:

$$\varepsilon = 1 - \frac{1 - \varepsilon_0}{1 - \varepsilon_0 \left[A \frac{P - P_a}{P} + (1 - A) \left(1 - \text{Exp} \left(-\frac{P - P_a}{B} \right) \right) \right]} \quad (18)$$

The parameters A and B can be determined from experimental data using curve fitting analysis. Application of the curve fitting analysis to the experimental data (Table III) based on this work provided the values of A and B of 0.7858 and 254.39, respectively, with an acceptable value of the coefficient of determination ($R^2 = 0.9931$) and a low value of

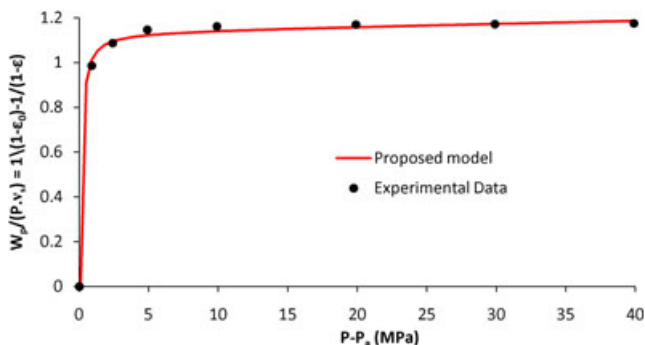


Fig. 5. Plot of experimental data in terms of porosity versus the applied pressure difference ($P - P_a$) according to Eq. (15).

the root mean square error (RMSE = 0.0115). Table V shows the predictive capability of the proposed model [Eq. (18)] for the rest of the experimental data from this work using these predetermined values of A and B . It shows that the proposed equation could predict the experimental values of open porosities by an average error of $\pm 3.09\%$.

To understand the porosity-pressure (uniaxial pressure) behavior of the applied ceramic powder (NiO/YSZ) at higher pressures, the proposed model [Eq. (18)] was applied using the predetermined values of A and B with the results shown in Fig. 6. Accordingly, three different regimes could be identified during the compaction process. At the first regime starting from the atmospheric pressure, a small increase in the applied uniaxial pressure caused a rapid quasi-linear decrease in porosity until the critical porosity (ε_0) was reached. Critical porosity corresponded to a small uniaxial pressure referred to here as the critical pressure (P_c). Beyond the critical pressure and by applying higher uniaxial pressures, the second regime was observed with a nonlinear dependency of porosity to pressure (uniaxial strength) until reaching a specific pressure called the transitional pressure (P_T). The transitional pressure for the proposed model corresponded to the inflection point of the curve (by logarithmic scale), equaling the value of the parameter B ($B = P_T$). Thus, the model used two dimensionless pressure groups (i.e., $\frac{P - P_a}{P}$ and $\frac{P - P_a}{B}$) as independent parameters to predict the porosity as a dimensionless dependent parameter, confirming that the model was supported by a valid dimensional analysis. In addition, it was found that the value of parameter A approximately corresponded to the estimated porosity at the transitional pressure divided by the skeletal specific volume of solid ($A \sim \frac{\varepsilon(P_T)}{v_s}$). By increasing the applied uniaxial pressure beyond the transitional pressure, the third pressure-porosity regime observed displayed another quasi-linear behavior. At the third pressure-porosity regime, a small change in porosity required a significant change in pressure, especially at the lower porosities. The outcomes (Fig. 6) were in agreement with the idealized uniaxial strength versus porosity configuration.^{53,54}

Table V. Prediction Ability of the Proposed Model [Eq. (18)]

Applied uniaxial pressure (MPa)	Experimental porosity, ε (%)	Predicted porosity, ε (%)	Error (%)
0	59.25	59.25	0.00
1	31.89	29.88	-6.28
2.5	26.87	26.19	-2.53
5	23.52	24.74	+5.17
10	22.62	23.73	+4.91
20	22.12	22.71	+2.66
30	22.02	21.92	-0.43
40	21.81	21.21	-2.74

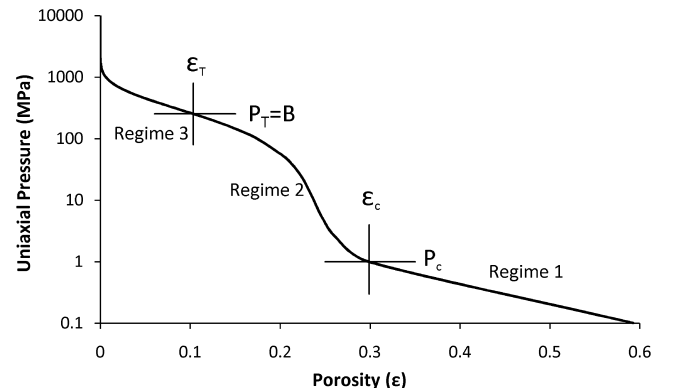


Fig. 6. Predicted uniaxial strength versus porosity for NiO/YSZ at higher pressures.

(B) *Effect of Pore-Former Blend Ratio and Size Ratio:* For the fabricated ceramic bodies, parameters such as blend ratio and particle size ratio of the pore-forming agent are the main factors affecting the final porosity. In general, adding a given amount of pore-forming agent creates additional porosity on top of the available intrinsic porosity of ceramic bodies. The intrinsic porosity is the porosity of the sintered ceramic material without the use of any pore-former. So, the final porosity of the sintered ceramic body can be expressed as:

$$\varepsilon = \varepsilon_i + \varepsilon_c \quad (19)$$

where ε_i and ε_c are the intrinsic- and the created-porosity, respectively. The blend ratio of pore-former is the primary influencing parameter to change the final porosity. Physically, adding any pore-former to increase the porosity must satisfy two boundary conditions. First, the final porosity must equal the intrinsic porosity as the blend ratio approaches zero, and secondly, the final porosity must equal 1 if the blend ratio approaches 1. These boundary conditions can be expressed as:

$$\lim_{\xi \rightarrow 0} \varepsilon = \varepsilon_i \quad (20)$$

$$\lim_{\xi \rightarrow 1} \varepsilon = 1 \quad (21)$$

Curve fitting analysis of the experimental data (Table IV) showed a relationship between the created porosity (ε_c) and the pore-former blend ratio (ξ) as follows:

$$\varepsilon_c = \frac{C_1}{\xi^2 + (\xi - C_2)\text{Ln}(\xi)} \quad (22)$$

where C_1 , and C_2 are the model coefficients. The coefficient C_1 can be estimated by substituting Eq. (22) into Eq. (19) and then using the second boundary condition [Eq. (21)] as follows:

$$\lim_{\xi \rightarrow 1} \varepsilon = \varepsilon_i + \frac{C_1}{\xi^2 + (\xi - C_2)\text{Ln}(\xi)} = 1 \quad (23)$$

Equation 23 implies that the value of parameter C_1 is equal $1 - \varepsilon_i$, and consequently the final porosity can be expressed as a function of the intrinsic porosity and the blend ratio by the following equation:

$$\frac{\varepsilon - \varepsilon_i}{1 - \varepsilon_i} = \frac{1}{\xi^2 + (\xi - C_2)\text{Ln}(\xi)} \quad (24)$$

Thus, Eq. (24) was used to fit the experimental data of this work (Table IV, all sets of data), with the goodness of fit summarized in Table VI. Equation (24) involved one model coefficient (C_2) that could be expressed as a function of the particle size ratio (λ). The size ratio as applied in the experiments and the physical boundary conditions were used to find the experimental correlation for coefficient C_2 :

$$C_2 = \frac{K}{\lambda^m} \quad (25)$$

In Eq. (25), k , and m are the model coefficients. Substituting Eq. (25) to Eq. (24) results in the final porosity correlation for the fabricated ceramic body as follows:

$$\frac{\varepsilon - \varepsilon_i}{1 - \varepsilon_i} = \frac{1}{\xi^2 + (\xi - \frac{K}{\lambda^m})\text{Ln}(\xi)} \quad (26)$$

Equation (26) was used to predict the experimental data of this work (Table IV), with the results shown in Fig. 7. The model coefficients and the goodness of fit statistic are reported in Table VII. The proposed model (Eq. 26) showed an acceptable consistency with the experimental data ($R^2 > 0.9975$ and $\text{RMSE} < 0.0075$). The model also complied with the physical boundary conditions for the blend ratio and the size ratio, for example, as the porosity took the value of intrinsic porosity (ε_i) when the size ratio or the blend ratio approached zero, i.e., when no pore-forming agent was added. For finite size ratios, the porosity took the value of 1 when the blend ratio approached 1, meaning that the solid mixture was entirely composed of pore-former (with no ceramic solid). For the case of similar particle size for pore-former and ceramic particles, parameter λ should equal 1 and consequently, Eq. (26) would take the form of Eq. (24).

(C) *Applications:* We also applied Eqs. (18) and (26) using appropriate data in literature covering different ranges of fabrication pressure, pore-former fractions, and particle size ratio. Tables VIII and IX summarized the goodness of fit and the predicted coefficients for different ceramic and nonceramic powders, demonstrating the versatility of the proposed models to predict the porosity for different ceramic and nonceramic powders. The reported values of R^2 and RMSE (averagely $R^2 > 0.99$ and $\text{RMSE} < 0.015$) in Tables VIII and IX demonstrates a relatively good predictive capability for the proposed models (Eqs. (18) and (26)).

Determining the significance of the processing parameters as investigated here would depend on the selected fabrication method. For example, if a fabricated ceramic body is made using the compression method (without pore-former), the main parameter is the applied uni-axial pressure, and Eq. (18) can be used to predict the final open porosity. On the other hand, if a ceramic body is made by compression or other methods using a pore-forming agent, at first, the intrinsic

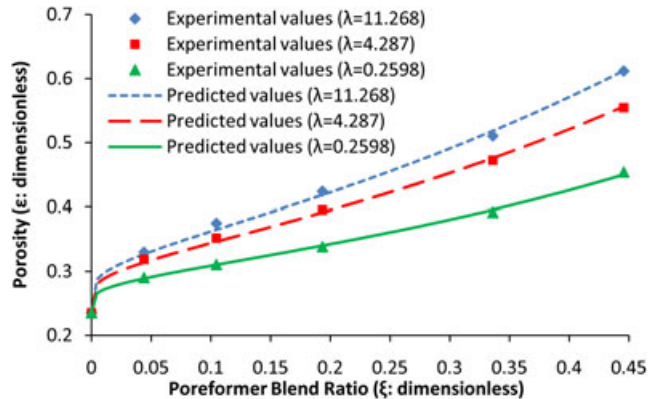


Fig. 7. Plots of porosity as a function of blend ratio and size ratio of the pore-former, fitted with Eq. (26).

Table VI. Model Coefficients and Goodness of Fit Data for the Fitted Curve on Volumetric Data [Eq. (24)]

Model coefficients and Goodness of fit	Particle size ratio		
	$\lambda = 11.268$	$\lambda = 4.287$	$\lambda = 0.2598$
C_2	2.7083	3.1450	4.5981
R^2	0.9975	0.9985	0.9985
RMSE	0.0067	0.0044	0.0029

Table VII. Model Coefficients and Goodness of Fit Data for the Proposed Model for Porosity [Eq. (26)]

Model coefficients and Goodness of fit	Particle size ratio		
	$\lambda = 11.268$	$\lambda = 4.287$	$\lambda = 0.2598$
K	10.791	8.6451	3.5300
m	0.5707	0.6946	0.1961
R^2	0.9975	0.9985	0.9985
RMSE	0.0075	0.0049	0.0033

Table VIII. Model Evaluation and Curve Fitting Results for Eq. (18) Using Literature Data

Ref.	Powder	Pressure range (MPa)	ϵ_0	A	B	R^2	RMSE
55	Electrolytic Copper	0–1000	0.700	0.6376	204.26	0.9965	0.0130
	Stainless Steel	0–926.1	0.626	0.5847	496.22	0.9961	0.0122
	Tungsten Carbide	0–864	0.799	0.7302	800.04	0.9859	0.0152
56	Zink Powder	0–450	0.620	0.7692	176.50	0.9948	0.0162
57	Mixture of Yttrium, Copper, and Barium oxides	0–350	0.910	0.9653	304.62	0.9963	0.0231
58	Calcium Phosphate cement PL2	0–175	0.575	0.4085	253.91	0.9905	0.0112
	Calcium Phosphate cement PL3		0.445	0.2340	413.31	0.9976	0.0040
59	SiC/ α -Alumina/Graphite	30–90	0.9723 [†]	0.9736	584.78	0.9988	0.0012
22	Ammonium Nitrate	1–19.6	0.7076 [†]	0.7626	10.156	0.9979	0.0064
	Potassium Chloride	1.2–76.9	0.8866 [†]	0.8905	27.173	0.9908	0.0158
	Potassium Nitrate	0.6–76.4	0.6617 [†]	0.6267	31.879	0.9881	0.0164

[†]Predicted value.

Table IX. Model Evaluation and Curve Fitting Results for Eq. (26) Using Literature Data

Ref.	Ceramic powder	Pore-former	λ	ϵ_i	K	m	R^2	RMSE
45	YSZ	Graphite	~40	0.431	14.079	0.3601	0.9988	0.0045
60	Alumina	PVAc	20 [†]	0.05	12.321	0.4382	0.9928	0.0127
42	α -Alumina	Corn starch	18	0.1107 [†]	13.439	0.4884	0.9992	0.0084
		Wheat starch	23.5	0.1636 [†]	15.410	0.4433	0.9975	0.0119
61	Alumina	Potato starch	81.6	0.1446 [†]	18.060	0.4053	0.9998	0.0028
		Corn starch	23.33	0.1235 [†]	14.409	0.4626	0.9958	0.0139
		Wheat starch	33.33	0.1165 [†]	16.220	0.4275	0.9954	0.0137
62	Alumina (78 wt%)	Corn starch	17.5	0.1869 [†]	14.009	0.4722	0.9955	0.0095

[†]Predicted value.

porosity should be measured experimentally (by mercury porosimetry or Archimedes technique), before applying Eq. (26) to predict the final porosity. It should be noted that as shown from Eq. (26), the blend ratio of a pore-former was more important compared with the size ratio in determining the final porosity of the ceramic bodies.

IV. Conclusions

This work detailed the development of porosity models for fabricated ceramic anode, phenomenologically developed as a function of the ceramic processing variables of the applied uni-axial pressure, the pore-former volumetric blend ratio, and the particle-size ratio. Experiments were conducted by preparing ceramic/pore-former blends comprising NiO/YSZ as the ceramic powder and CMSs (carbon microspheres) as the pore-forming agent, using a range of solid volume fractions of the pore-former and diameters of the CMSs. We also investigated the effects of fabrication pressure, by measuring the open porosities of the prepared samples to determine the porosity behavior of the sintered ceramic substrates. The applied uni-axial pressure as the main fabrication parameter and the blend ratio of CMS significantly influenced the porosity of the final ceramic body, whereas the proposed models could potentially be used to predict the porosity of porous bodies from ceramic and nonceramic powders.

Acknowledgments

The authors acknowledge the technical support from Monash Center for Electron Microscopy. This work was supported by the Australian Research Council. Huanting Wang thanks the Australian Research Council for a Future Fellowship (FT100100192).

References

- R. W. Rice, *Porosity of Ceramics*. Marcel Dekker, New York, 1998.
- R. McPherson, "A Review of Microstructure and Properties of Plasma Sprayed Ceramic Coating," *Surf. Coat. Technol.*, **39/40** [1] 173–81 (1989).
- R. W. Rice, "Effects of Inhomogeneous Porosity on Elastic Properties of Ceramics," *J. Am. Ceram. Soc.*, **58** [9–10] 58–9 (1975).
- R. W. Rice, "Evaluating Porosity Parameters for Porosity-Property Relations," *J. Am. Ceram. Soc.*, **76** [7] 1801–8 (1993).
- J. J. Haslam, A. Q. Pham, B. W. Chung, J. F. Di Carlo, and R. S. Glass, "Effects of the Use of Pore Formers on Performance of an Anode Supported Solid Oxide Fuel Cell," *J. Am. Ceram. Soc.*, **88** [3] 513–8 (2005).
- J. Kim, A. V. Virkar, K. Fung, K. Mehta, and S. C. Singhal, "Polarization Effects in Intermediate Temperature, Anode-Supported Solid Oxide Fuel Cells," *J. Electrochem. Soc.*, **146** [1] 69–78 (1999).
- A. Sanson, P. Pinasco, and E. Roncari, "Influence of Pore Formers on Slurry Composition and Microstructure of Tape Cast Supporting Anodes for SOFCs," *J. Eur. Ceram. Soc.*, **28** [6] 1221–6 (2008).
- R. M. C. Clemmer and S. F. Corbin, "Influence of Porous Composite Microstructure on the Processing and Properties of Solid Oxide Fuel Cell Anodes," *Solid State Ionics*, **166** [3–4] 251–9 (2004).
- J. Hu, Z. Lu, K. Chen, X. Huang, N. Ai, X. Du, C. Fu, J. Wang, and W. Su, "Effect of Composite Pore-Former on the Fabrication and Performance of Anode-Supported Membranes for SOFCs," *J. Membr. Sci.*, **318** [1–2] 445–51 (2008).
- A. C. Müller, D. Herbstritt, and E. Ivers-Tiffée, "Development of a Multi-layer Anode for Solid Oxide Fuel Cells," *Solid State Ionics*, **152–153**, 537–42 (2002).
- S. C. Singhal and K. Kendall, *High Temperature Solid Oxide Fuel Cells: Fundamentals Design and Applications*. Elsevier, Oxford, 2003.
- A. V. Virkar, J. Chen, C. W. Tanner, and J. Kim, "The Role of Electrode Microstructure on Activation and Concentration Polarizations in Solid Oxide Fuel Cells," *Solid State Ionics*, **131** [1–2] 189–98 (2000).
- H. Yakabe, M. Hishunuma, M. Uratani, Y. Matsuzaki, and I. Yasuda, "Evaluation and Modeling of Performance of Anode-Supported Solid Oxide Fuel Cell," *J. Power Sources*, **86** [1–2] 423–31 (2000).
- C. L. Tsai and V. H. Schmidt, "Tortuosity in Anode-Supported Proton Conductive Solid Oxide Fuel Cell Found from Current Flow Rates and Dusty-Gas Model," *J. Power Sources*, **196** [2] 692–9 (2011).
- A. Konno, H. Iwai, M. Satio, and H. Yoshida, "A Corrugated Mesoscale Structure on Electrode-Electrolyte Interface for Enhancing Cell Performance in Anode-Supported SOFC," *J. Power Sources*, **196** [18] 7442–9 (2011).
- R. W. Rice, *Mechanical Properties of Ceramics and Composites: Grain and Particle Effects*. Marcel Dekker, New York, 2000.
- E. Chevalier, D. Chulia, C. Pouget, and M. Viana, "Fabrication of Porous Substrates: A Review of Processes Using Pore Forming Agents in the Biomaterial Field," *J. Pharm. Sci.*, **97** [3] 1135–54 (2008).
- E. Gregorová and W. Pabst, "Porous Ceramics Prepared Using Poppy Seed as a Pore-Forming Agent," *Ceram. Int.*, **33** [7] 1385–8 (2007).
- A. I. Ratko, A. I. Ivantes, and S. M. Azarov, "Effect of Additives on the Pore Structure of Ceramics Based on Crystalline SiO₂," *Inorg. Mater.*, **44** [7] 778–84 (2008).
- W. Chen and S. G. Malghan, "Investigation of Compaction Equations for Powders," *Powder Technol.*, **81** [1] 75–81 (1994).
- P. J. Denny, "Compaction Equations: A Comparison of the Heckel and Kawakita Equations," *Powder Technol.*, **127** [2] 162–72 (2002).

- ²²E. E. Walker, "The Properties of Powders. Part VI. The Compressibility of Powders," *Trans. Faraday Soc.*, **19**, 73–82 (1923).
- ²³R. Panelli and F. A. Filho, "A Study of a New Phenomenological Compacting Equation," *Powder Technol.*, **114** [1–3] 255–61 (2001).
- ²⁴R. W. Heckel, "Density-Pressure Relationships in Powder Compaction," *Trans. Metall. Soc. AIME*, **221**, 671–5 (1961).
- ²⁵K. Kawakita and K. H. Lüdde, "Some Considerations on Powder Compression Equations," *Powder Technol.*, **4** [2] 61–8 (1971).
- ²⁶C. A. Bruch, "Problems in Die-Pressing Submicron Size Alumina Powder," *Ceram. Age*, **83** [10] 44–53 (1967).
- ²⁷H. M. MacLeod, "Compaction of Ceramics"; pp. 241–76 in *Enlargement and Compaction of Particulate Solids*, Edited by N. G. Stanley-Wood. Butterworths, London, 1983.
- ²⁸M. Celik, "Overview of Compaction Data Analysis Techniques," *Drug Dev. Ind. Pharm.*, **18** [6–7] 767–810 (1992).
- ²⁹J. M. Sonnergaard, "A Critical Evaluation of the Heckel Equation," *Int. J. Pharm.*, **193** [1] 63–71 (1999).
- ³⁰J. M. Dalla Valle, *Micromeritics*. Pitman Publishing Corp., New York, 41–67, 1948.
- ³¹A. R. Cooper Jr. and L. E. Eaton, "Compaction Behavior of Several Ceramic Powders," *J. Am. Ceram. Soc.*, **45** [3] 97–101 (1962).
- ³²C. L. Huffine and C. F. Bonilla, "Particle-Size Effects in the Compression of Powders," *AIChE J.*, **8** [4] 490–3 (1962).
- ³³J. T. Fell and J. M. Newton, "Effect of Particle Size and Speed of Compaction on Density Changes in Tablets of Crystalline and Spray-Dried Lactose," *J. Pharm. Sci.*, **60** [12] 1866–9 (1971).
- ³⁴P. York, "Particle Slippage and Rearrangement During Compression of Pharmaceutical Powders," *J. Pharm. Pharmacol.*, **30** [1] 6–10 (1978).
- ³⁵J. Zheng, W. B. Carlson, and J. S. Reed, "Dependence of Compaction Efficiency in Dry Pressing on the Particle Size Distribution," *J. Am. Ceram. Soc.*, **78** [9] 2527–33 (1995).
- ³⁶M. Djuric, R. M. Neducin, J. Ranogajec, and M. Radeka, "Particle Size Range as a Factor Influencing Compressibility of Ceramic Powder," *Ceram. Int.*, **21** [4] 227–30 (1995).
- ³⁷A. B. Yu and Z. H. Gu, "Characterization of the Porosity-Pressure Relation of Cohesionless Powders," *Adv. Powder Technol.*, **4** [3] 199–216 (1993).
- ³⁸A. Balakrishnan and C. L. Martin, "Modeling of Compaction and Green Strength of Aggregated Ceramic Powders," *J. Am. Ceram. Soc.*, **94** [4] 1046–52 (2011).
- ³⁹D. M. Liu, "Influence of Solid Loading and Particle Size Distribution on the Porosity Development of Green Alumina Ceramic Mouldings," *Ceram. Int.*, **23** [6] 513–20 (1997).
- ⁴⁰J. Divisek, R. Wilkenhoener, and Y. Volkovich, "Structure Investigations of SOFC Anode Cermets. Part I: Porosity Investigations," *J. Appl. Electrochem.*, **29** [2] 153–63 (1999).
- ⁴¹S. F. Corbin, J. Lee, and X. Qiao, "Influence of Green Formulation and Pyrolyzable Particulates on the Porous Microstructure and Sintering Characteristics of Tape Cast Ceramics," *J. Am. Ceram. Soc.*, **48** [1] 41–7 (2001).
- ⁴²E. Gregorova, Z. Zivcova, and W. Pabst, "Starch as a Pore-Forming and Body-Forming Agent in Ceramic Technology," *Starch/Stärke*, **61** [9] 495–502 (2009).
- ⁴³L. Mingyi, Y. Bo, X. Jingming, and C. Jing, "Influence of Pore Formers on Physical Properties and Microstructures of Supporting Cathodes of Solid Oxide Electrolysis Cells," *Int. J. Hydrogen Energy*, **35** [7] 2670–4 (2010).
- ⁴⁴Q. Wang, H. Li, L. Chen, and X. Huang, "Monodispersed Hard Carbon Spherules with Uniform Nanopores," *Carbon*, **39** [14] 2211–4 (2001).
- ⁴⁵M. Boaro, J. M. Vohs, and R. J. Gorte, "Synthesis of Highly Porous Ytria-Stabilized Zirconia by Tape-Casting Methods," *J. Am. Ceram. Soc.*, **86** [3] 395–400 (2003).
- ⁴⁶E. Gregorova, W. Pabst, and I. Bohacenko, "Characterization of Different Starch Types for Their Application in Ceramic Processing," *J. Eur. Ceram. Soc.*, **26** [8] 1301–9 (2006).
- ⁴⁷S. W. Jung, J. M. Vohs, and R. J. Gorte, "Preparation of SOFC Anodes by Electrodeposition," *J. Electrochem. Soc.*, **154** [12] B1270–5 (2007).
- ⁴⁸M. Kim, J. Lee, and J. H. Han, "Fabrication of Anode Support for Solid Oxide Fuel Cell Using Zirconium Hydroxide as a Pore Former," *J. Power Sources*, **196** [5] 2475–82 (2011).
- ⁴⁹P. Lamy, G. Thomas, L. Brunet, and R. Erre, "Modelling the Porosity Evolution of a Powder Under Uniaxial Compression," *Propellants, Explosives, Pyrotechnics*, **30** [6] 397–403 (2005).
- ⁵⁰P. A. Webb, *Volume and Density Determinations for Particle Technologists*. Micromeritics Instrument Corporation, Norcross, Georgia, 2001.
- ⁵¹J. Van der Zwan and C. A. M. Siskens, "The Compaction and Mechanical Properties of Agglomerated Materials," *Powder Technol.*, **33** [1] 43–54 (1982).
- ⁵²M. Duberg and C. Nystrom, "Studies on Direct Compression of Tablets: XVII. Porosity Pressure Curves for the Characterisation of Volume Reduction Mechanisms in Powder Compression," *Powder Technol.*, **46** [1] 67–75 (1986).
- ⁵³L. Li and M. Aubertin, "A General Relationship Between Porosity and Uniaxial Strength of Engineering Materials," *Can. J. Civ. Eng.*, **30** [4] 644–58 (2003).
- ⁵⁴M. Aubertin, L. Li, R. Simon, and B. Bussière, A General Plasticity and Failure Criterion for Materials of Variable Porosity. Technical Report EPM-RT-2003-11, École Polytechnique de Montréal (2003).
- ⁵⁵G. Rong-De, "A new Powder Compaction Equation," *Int. J. Powder Metall.*, **27** [3] 211–6 (1991).
- ⁵⁶P. J. James, "Particle Deformation During Cold Isostatic Pressing of Metal Powders," *Powder Metall.*, **20**, 199–204 (1977).
- ⁵⁷S. Salib and C. Vipulanandan, "Property-Porosity Relationships for Polymer-Impregnated Superconducting Ceramic Composite," *J. Am. Ceram. Soc.*, **73** [8] 2323–9 (1990).
- ⁵⁸K. Ishikawa and K. Asaoka, "Estimation of Ideal Mechanical Strength and Critical Porosity of Calcium Phosphate Cement," *J. Biomed. Mater. Res.*, **29** [12] 1537–43 (1995).
- ⁵⁹S. Ding, S. Zhu, Y. P. Zeng, and D. Jiang, "Fabrication of Mullite-Bonded Porous Silicon Carbide Ceramics by In Situ Reaction Bonding," *J. Eur. Ceram. Soc.*, **27** [4] 2095–102 (2007).
- ⁶⁰T. Isobe, Y. Kameshima, A. Nakajima, and K. Okada, "Preparation and Properties of Porous Alumina Ceramics with Uni-Directionally Oriented Pores by Extrusion Method Using a Plastic Substance as a Pore Former," *J. Eur. Ceram. Soc.*, **27** [1] 61–6 (2007).
- ⁶¹E. Gregorova and W. Pabst, "Porosity and Pore Size Control in Starch Consolidation Casting of Oxide Ceramics-Achievements and Problems," *J. Eur. Ceram. Soc.*, **27** [2–3] 669–72 (2007).
- ⁶²E. Gregorova and W. Pabst, "Process Control and Optimized Preparation of Porous Alumina Ceramics by Starch Consolidation Casting," *J. Eur. Ceram. Soc.*, **31** [12] 2073–81 (2011). □